Accelerated Electrochemical Machining Tool Design via Multiphysics Modeling

B. Skinn[a], T. D. Hall[a], S. Snyder[a], K. P. Rajurkar[b], and E.J. Taylor[a]

[a] Faraday Technology, Inc., Englewood, Ohio 45315, USA
[b] Department of Mechanical & Materials Engineering, University of Nebraska – Lincoln, Lincoln, Nebraska 68588, USA

A significant challenge preventing wider industrial adoption of electrochemical machining (ECM) is the lack of efficient, *a priori* means for selection of a tool design to achieve a target part shape with high accuracy. Tight coupling among the numerous physical phenomena active in industrial electrochemical processes confounds the simplification approaches available in other contexts. Recent developments in computational hardware and software allow simultaneous solution of the relevant governing equations, potentially enabling practical tool design methods by solution of the "inverse electric field problem." This paper discusses recent work comparing primary current distribution simulations to indentations fabricated by ECM of steel panels. Good agreement was obtained for a subset of the tests performed. The results highlight the importance of including additional physical phenomena such as flow effects and electrochemical polarization in order to obtain more accurate simulations. In particular, the current efficiency of the metal dissolution reaction likely must be considered.

Introduction

Electrochemical machining (ECM) is a manufacturing technology that allows metal to be precisely removed by electrochemical oxidation and dissolution into an electrolyte solution. As illustrated in Figure 1, after McGeough (1), the workpiece is the anode and the tool is the cathode in an electrochemical cell. By relative movement of the shaped tool into the workpiece, the mirror image of the tool is "copied" or machined into the workpiece. Compared to mechanical or thermal machining processes where metal is removed by cutting or electric discharge/laser machining, respectively, ECM does not suffer from tool wear or result in a thermally damaged surface layer on the workpiece. Consequently, ECM has strong utility as a manufacturing technology for fabrication of a wide variety of metallic parts and components, and includes machining, deburring, boring, radiusing and polishing processes.

As described previously (2), ECM has numerous advantages relative to traditional machining including i) applicability to hard and difficult to cut materials, ii) no tool wear, iii) high material removal rate, iv) smooth bright surface finish, and v) production of parts with complex geometry. In spite of these advantages, five research challenges were noted as preventing the wider adoption of ECM, i) disposal of machining products, ii) electrolyte processing, iii) tool design, iv) machining accuracy, and v) process

monitoring and control. In the sixteen years since these challenges were issued, process monitoring and control [challenge (v)] are no longer a major difficulty due to advancements in sensors and automation. Consistent with conservation principles regarding management of natural (metals, water, energy) resources, such as the "Net Zero" vision of the U.S. Army (3), Faraday has recently developed a patent-pending process (4) which recovers metals, recycles electrolyte and reduces water usage. This process addresses two of the remaining four research challenges, (i) sludge disposal and (ii) electrolyte processing (5). The work described herein is a first step toward addressing the final two challenges: (iii) tool design and (iv) machining accuracy.

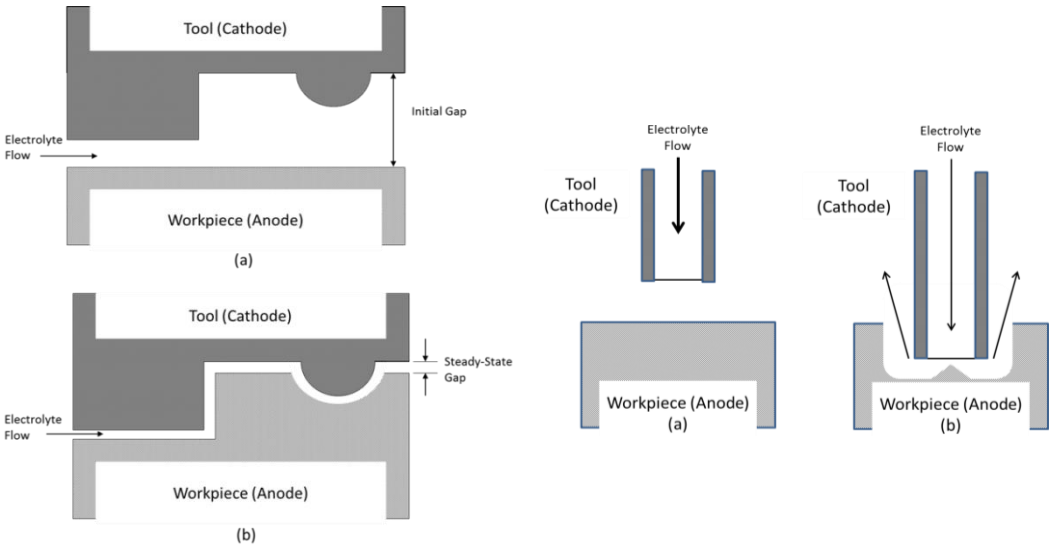

Figure 1. Initial (a) and final (b) tool/workpiece configurations in "cross-flow" (left) and "flow-through" (right) ECM.

Modeling of ECM

Electrochemical machining (ECM) is a material removal process whereby the workpiece is the anode and the tool is the cathode in an electrochemical cell. The material removal is governed by Faraday's laws of electrolysis and at a high level can be generally represented by reaction [1]:

$$\mathrm{M} \rightarrow \mathrm{M}^{z+} + z\mathrm{e}^{-}, \qquad [1]$$

where "M" is the (typically metallic) material being machined and z is the valence of the material. According to Faraday's laws of electrolysis (6), the mass m of material removed is:

$$m = (A * I * t)/(z * F). \qquad [2]$$

Correspondingly, the volume v of material removed is:

$$v = (A * I * t)/(z * F * \rho), \qquad [3]$$

where in both expressions A is the atomic weight, I is the current, t is the time over which the current is applied, F is Faraday's constant, and ρ is the density of the material.

Consequently, in theory, the amount of material removed in ECM is simply controlled by the current, processing duration, and material-specific attributes.

However, in practice the ECM process is much more complicated. Specifically, the workpiece anodic electrochemistry is complicated by a competing side reaction of oxygen evolution:

$$2\,H_2O \rightarrow O_2 + 4\,H^+ + 4\,e^- \qquad [4]$$

The tool electrode (cathode) reaction is primary hydrogen evolution:

$$4\,H_2O + 4\,e^- \rightarrow 2\,H_2 + 4\,OH^- \qquad [5]$$

Oxygen evolution (reaction [4]) at the workpiece is a competing reaction with the desired metal dissolution (reaction [1]) there. The current efficiency of the ECM process is defined as the fraction of total current going to the desired anodic workpiece dissolution reaction.

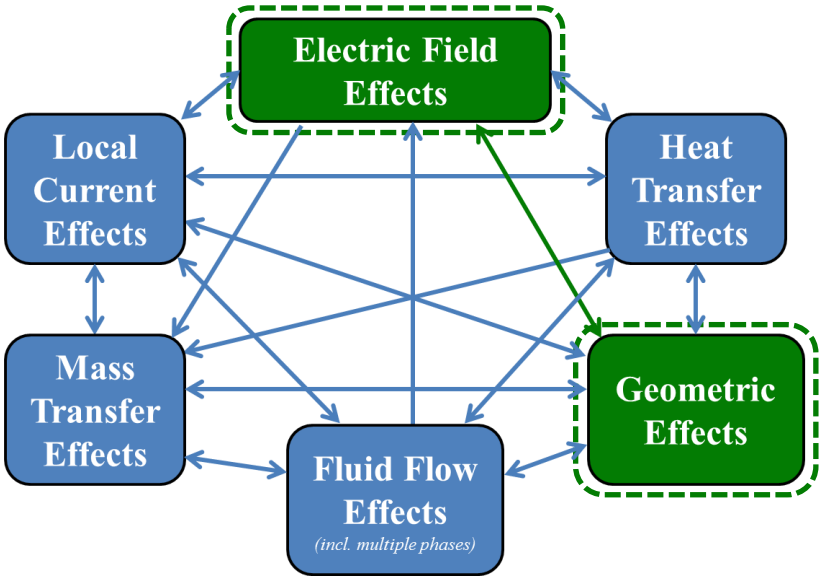

Figure 2. Physical phenomena encountered in ECM. The two phenomena marked with dashed outlines are those included in the simulations performed in this work (*vide infra*).

One of the challenges in modeling industrial electrochemical processes is the tight coupling among several key physical phenomena, which confounds the simplification approaches available for other classes of electrochemical problems. As partially illustrated in Figure 2, interrelationships between many phenomena impact the ECM process. These phenomena include i) the electric field, ii) concentration profiles of reactants and products, iii) heat generation/transfer, iv) fluid mechanics, v) heterogeneous and homogeneous reactions, and vi) the local and overall geometry of the workpiece and tool. Despite the complications of the coupled physics, the governing equations themselves are relatively straightforward, albeit not concise (7,8). For example, in ECM processing of non-passivating materials which do not form a strong oxide film, the electrolytes used are generally simple salts such as sodium chloride or sodium nitrate. Based on their electrochemical polarization behavior (i.e., current versus potential

relationship) for steel, however, sodium nitrate and sodium chloride are generally characterized as passivating and non-passivating electrolytes, respectively. Practically speaking, this means that the ECM current efficiency is generally higher for the sodium chloride electrolyte than sodium nitrate electrolyte. However, the anisotropy of the material removal is generally better (i.e., less material is removed in the lateral direction per unit depth machined) for the sodium nitrate electrolyte. Thus, the choice of the ECM electrolyte itself embodies a coupling between the electrochemical phenomena occurring at the part surface and the macroscopic material removal profile observed in ECM operations.

In general, the practical implications of these coupled physics are varied. The generation of bubbles and dissolved or precipitated metal species within the inter-electrode gap (IEG) impacts the electrolyte pressure drop, temperature, conductivity, and fluid flow profile, as well as influencing the form of the electric field between the electrodes. All of these properties are in turn strongly dependent on IEG dimensions and electrolyte flow (9). These flow-dependent variations from the electrolyte inlet to outlet impact the local voltage polarization across the IEG and electrochemical reactions occurring at each electrode. Joule heating from the passed electrical current can cause localized increases in the electrolyte and/or electrode temperature, further altering the position-dependent behavior of the process. Finally, a strong dependence on time can be expected in all of the above interactions, since the gross form of the workpiece changes due to material dissolution, and the spatial distribution of the localized variations in multiphysics properties evolves accordingly.

In spite of the complex interactions of these physical phenomena, ECM multiphysics simulations of electric razor blades (10) and jet engine turbine blades (8) have recently been reported. Unlike prior simulations of electrochemical deposition or plating, these simulations use an "inverted simulation strategy" where the desired workpiece target geometry is used to calculate the tool geometry effectively by inverting a typical electric field calculation. In this work, preliminary feasibility for a similar multiphysics-based "inverted-solution" design platform to predict optimal ECM tool shape using commercially available multiphysics simulation software has been demonstrated in conjunction with well-defined validation experiments. The feasibility demonstration includes matched experiments and simulations with two electrolyte flow/tool geometries, termed "cross-flow" and "flow-through", as depicted in Figure 1.

Materials and Methods

Apparatus

Tool Automation and Electrolyte Handling. In order to provide accurate control of the ECM tool position, an automated drive assembly and mounting apparatus was fabricated. The completed apparatus and selected components are shown in Figure 3A. The drive train was a backlash-free ball-screw glide track (EGSK-33-100-6P, Festo Group, Hauppage, NY, USA) driven by a high-resolution stepper motor (EMMS-AS-40-S-LS-TM, Festo) with reducing gearing (PLE40-060-SSSA3AA-Y8/25/3, Neugart USA Corp, Charlotte, NC, USA) to enable the slow tool advancement rates used in the ECM tests. All drive train components were procured from Monarch Automation (West Chester, OH, USA). The motor, gearing and drive were supported by a PVC brace, and the brass tool

was anchored by a conductive extension bar to the nonconductive Garolite stage adapter plate. The tool was precision-driven into the flow module by the motor, after affixing the flow module to an ECM part (see below). The baseplate was designed to provide alignment and structural support to the overall assembly during processing. The processing electrolyte was prepared from technical grade NaCl or $NaNO_3$, as appropriate (Chemical Services, Dayton, OH, USA), and was delivered into the IEG via a centrifugal pump. Precipitated iron oxide-hydroxide sludge was removed from the electrolyte by filtration in a separate fluidic circuit.

Flow Module. A flow module was designed in the SolidEdge 3-D CAD software package (Siemens PLM Software, Plano, TX, USA) to encapsulate the active ECM region of the system. A close-up photograph of the final flow module, fabricated by 3-D printing in glass-filled nylon (Stratasys Ltd., Valencia, CA, USA), is provided as Figure 3B. Total module dimensions were 2.5″ W × 2.5″ L × 1.5″ H. The central hole i.d. was approximately $^{5}/_{16}$″, to accommodate the plastic insulating layer around the o.d. of the ¼″ rod and tube tools. One of the two ports with $^{1}/_{8}$″ NPT threading for fluidic connections is visible just below center-frame in Figure 3B. Four counter-bored holes at the corners of the chamber were used to secure it to the ECM workpiece, as described below. Figure 4 schematizes the flow configurations for the tube and rod tools that were used in the ECM tests.

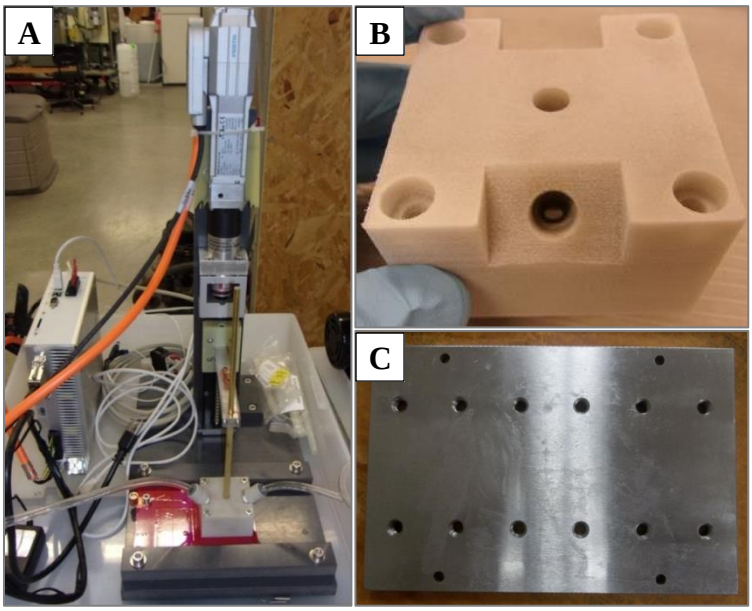

Figure 3. (A) Photograph of the fully commissioned ECM apparatus, with rod tool, motor controller, and fluidic connections to the flow module. Close-up photographs of (B) the 3-D printed flow module and (C) an alloy steel ECM part.

ECM Part. The parts machined in the ECM tests were flat plates (Figure 3C), sized to accommodate the geometric and load limits of the stage of a Nanovea ST-400 optical profilometer (Irvine, CA, USA). Five parts were fabricated, to enable simultaneous processing of one part while profilometric analysis of a previous part was underway. Each part had four mounting positions for the ECM flow module, which provided a total of forty available positions (five parts × four positions × two sides) for ECM processing. The four smaller holes were through-holes for mounting to the ST-400 stage, and the

larger holes were tapped and spaced to align with the counter-bored holes of the flow module.

ECM Tests

Seven ECM tests were conducted under DC potentiostatic control, with a variety of experimental parameters (see Table I). The response current was recorded at regular intervals during each test, to permit comparison with primary current distribution simulation predictions. The target run time for all tests was set at 20 min; Tests #2, #6 and #7 were stopped early due to contact between the tool and the part, as diagnosed by a sudden rise in the response current to the threshold programmed into the rectifier. Due to unanticipated throttling from small orifices in the quick-connect fittings used for the flow module ports, the pumping flow rate through the system was not measurable by the flowmeter installed in the system. The flow rates were thus the uncontrolled maximum values possible with the apparatus as constructed. The NaCl and $NaNO_3$ electrolytes were prepared at concentrations of 100 g L^{-1} and 180 g L^{-1}, respectively, providing equal conductivities of 140 mS cm^{-1}. Sodium chloride and sodium nitrate were selected as model electrolytes embodying "active" (more isotropic, faster machining) and "passive" (more anisotropic, slower machining) ECM behavior, respectively, as noted above. In all tests performed with a moving tool, minor challenges were encountered in achieving smooth travel of the tool through the bore hole of the flow module, due to the tool catching slightly along the inner diameter of the bore. Minor electrolyte seepage also occurred between the tool and the wall of the bore hole. Both of these observations indicate that re-development of the flow module would be needed for future work with this tooling configuration.

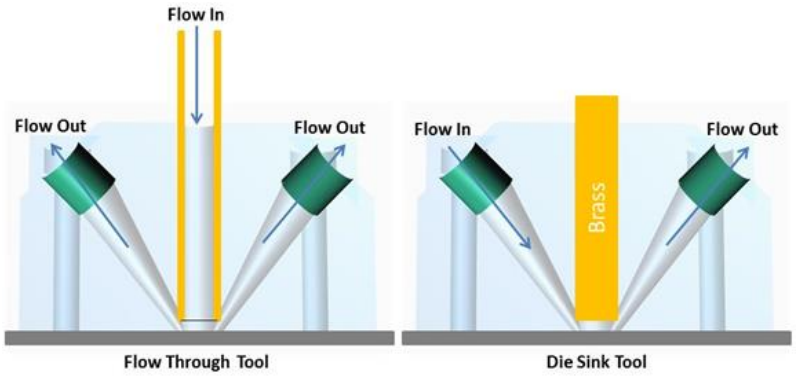

Figure 4. 3-D CAD drawings of the flow assembly with tube (flow-through, left) and rod (cross-flow, right) tools indicated.

Test #1 was run as an initial test of the electrical and flow subsystems, to confirm that material could actually be machined from a part, and that the sludge formed could be cleared sufficiently from the IEG. The apparatus worked satisfactorily, machining approximately 1.7 mm (0.067″) into the surface of the part at the deepest point of material removal. Test #2 was run as a shakedown test of the tool drive automation hardware in conjunction with flow and electrochemical material removal. As noted above, in this test, the 0.012″ min^{-1} advancement rate was too great for the 0.050″ initial IEG and 5 V_{DC} applied potential, as the tool contacted the part at approximately 4.3 min into the run. A satisfactory machined profile was still obtained.

Test #3 represented an adjustment to both the applied voltage (and thus the material removal rate) as well as the tool advancement rate, in an effort to ensure a full 20-min test could be completed without collision of the tool into the part. This effort was successful; no collision was observed throughout the test, and based on the applied advancement rate and duration the tip of the tool should have been 0.045″ below the original surface of the part at the end of the test.

Table I: Experimental parameters for the ECM tests performed.

Parameter	Units	Run #1	#2	#3	#4	#5	#6	#7
Tool	–	Rod	Rod	Rod	Tube	Rod	Rod	Tube
Electrolyte	–	NaCl	NaCl	NaCl	NaCl	NaCl	$NaNO_3$	$NaNO_3$
V_{DC}	V	5	5	15	10	10	10	10
v_{tool}	mil min^{-1}	–	12	6	6	6	6	6
δ_o	mil	50	50	75	75	75	75	75
Δt	min	20	4.3	20	20	20	16	14

With the preliminary information in hand from tests #1 through #3, a standard set of operating conditions was selected for the remaining four tests (#4 through #7). One test each was performed with the four various combinations of the rod/tube tools and the NaCl/$NaNO_3$ electrolytes. The machined indentations were all photographed and scanned by optical profilometry, and the four standardized tests (#4 through #7) and one preliminary test (#2) were compared to primary current distribution simulation results (*vide infra*).

Primary Current Distribution Simulations

The simulations conducted for comparison to the historical and current ECM tests were specifically constructed to incorporate the minimum physics needed to describe the ECM process, using the COMSOL (Burlington, MA, USA) Multiphysics® software package. In particular, they included only the primary current distribution (geometrical effects) within the IEG and the resulting geometric deformations from material removal. All other phenomena were neglected, such as: i) electrochemical surface polarization; ii) resistive residues developed/retained on the part and/or tool surfaces; iii) local electrolyte saturation effects at the part surface; and iv) localized resistance from bubble generation. To note, given the known differences in ECM behavior of the NaCl and $NaNO_3$ electrolytes chosen (6,11), it was expected that the simple primary current distribution model used in these simulations would not be able to accurately model both electrolytes. However, as borne out by the results (*vide infra*), a quality match between model and experiment was obtained for a subset of the tests performed.

Square Cross-Flow Tool. As a preliminary effort, primary current distribution simulations were performed that aimed to approximate the processing conditions of an indentation (Figure 5, bottom left, boxed) processed with a rectangular tool (2 mm × 2 mm cross-section; Figure 5, top left) in a prior collaborative activity with a manufacturer of integrally-bladed rotors (IBRs). The model domain used for these simulations is shown in Figure 5 (right), where both the bottom face and sides of the tool were electrochemically active, along with the entire face of the part. A 10 mm L × 10 mm W × 4 mm H simulation domain was used without any optimization or sensitivity

analysis of the domain extents. An electrolyte conductivity of 100 mS cm^{-1} was assumed, which is representative for electrochemical processing of this type (4,5). A DC operating potential of 3 V was assumed for the simulation, which was selected to approximate the average effective potential of the pulse-reverse waveform actually used in machining the part. The initial IEG was 0.005″, with a constant downward tool driving rate of 0.0002″ s^{-1} (0.012″ min^{-1}). The simulation was run to a final time of 15 min, with simulation data stored for analysis every 0.3 min (18 s).

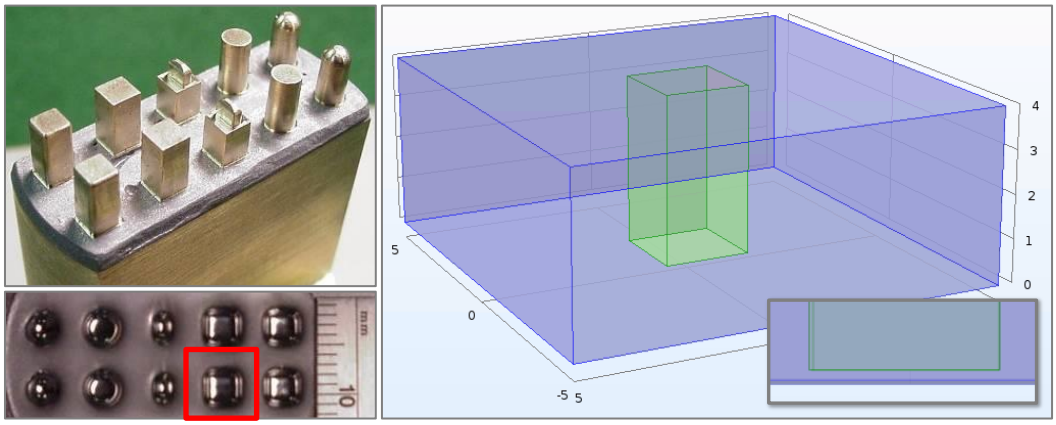

Figure 5. ECM tool (upper left) and machined part (lower left) from a prior ECM activity with an IBR manufacturer. Model geometry (right) for the boxed indentation, showing the 0.005″ initial IEG (inset, right).

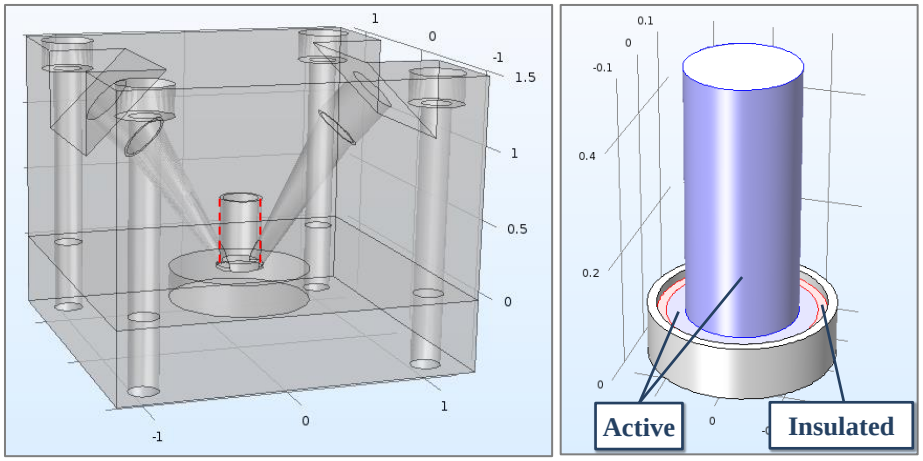

Figure 6. Model geometries used to simulate ECM trials in the cross-flow/rod-tool (left) and flow-through/tube-tool (right) configurations. The insulation on the o.d. of the rod tool is indicated by the dashed lines (see text).

Rod Cross-Flow Tool. In order to model the experimental ECM indentations a model geometry for the cross-flow/rod tool configuration was constructed using the SolidEdge 3-D CAD drawing of the flow module as a starting point. The final geometry used for the simulations is shown in Figure 6 (left). The vertical extent of the tool was reduced to include only a small section in the internal region of the flow module, so as to reduce the computational demand of modeling the thin shell of electrolyte between the insulated o.d. of the rod tool and the flow module (dashed lines), since the final machined profiles are

anticipated to be negligibly sensitive to this region of the system. The angled, tapered flow channels are visible on either side of the ECM-active region, though no flow effects were included in the simulations and the influence of these channels on the ECM profiles is anticipated to be minimal even in the presence of flow effects. The cylindrical region visible within the part is a "virtual" subdivision of the geometry, which was included to enable definition of higher- and lower-resolution regions of the finite element meshing within the part, since negligible changes in the geometry of the part should occur in locations sufficiently far from the active ECM region.

Tube Flow-Through Tool. A 3-D view of the model used to simulate the tests with the tube tool is shown in Figure 6 (right). Unlike with the model of the rod tool, only the electrolyte volume itself was modeled. The face and entire i.d. of the tube tool were modeled as electrochemically active; as with the rod tool, the insulation around the o.d. of the tool was explicitly included in the model.

Results and Discussion

Line profiles were extracted from all optical profilometry scans performed, for comparison to the primary current distribution simulation results. For the ECM tests performed with the rod and tube tools, appreciable asymmetry in the machined indentations was observed, and therefore profiles were extracted both perpendicular and parallel to the direction of flow.

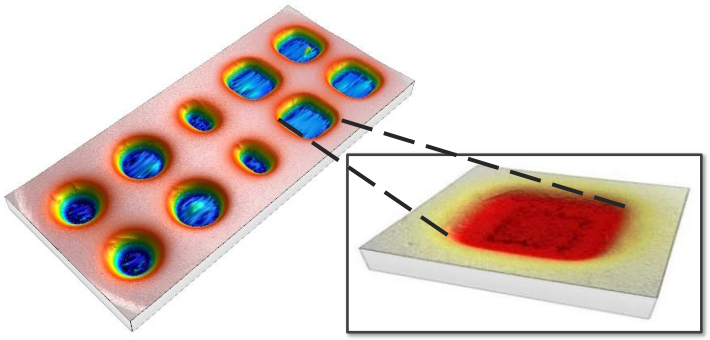

Figure 7. Low- and high-resolution scans of the part machined in the prior ECM collaboration with an IBR manufacturer.

Optical Profilometry

Square Cross-Flow Tool. Figure 7 shows an optical profilometric scan of the entire part of Figure 5 (bottom left), along with a high-resolution scan of just the indentation made by the square tool. Profiles taken perpendicular and parallel to the long dimension of the part were substantially similar, so a profile parallel to the long dimension was used below in comparisons with the primary current distribution simulation results.

Rod and Tube Tools. Photographs and optical profilometry scans of the seven indentations fabricated as described above are presented in Figures 8 and 9. The indentations obtained in tests #3 through #5 with the NaCl electrolyte were considerably asymmetric, perhaps due to irregular iron oxide-hydroxide accumulation within the IEG,

or to locally variable accumulation of residues on the part surface due to the shear stress distribution across the surface. Interestingly, the indentations formed using the $NaNO_3$ electrolyte (tests #6 and #7) were generally more axisymmetric, albeit exhibiting a somewhat more textured surface. The greater anisotropy of etch observed with the NaCl electrolyte is likely due to its greater "activity" as compared to $NaNO_3$ in ECM processing of steel: regions with locally reduced coverage of processing residues likely were machined proportionally faster in the "more active" NaCl electrolyte.

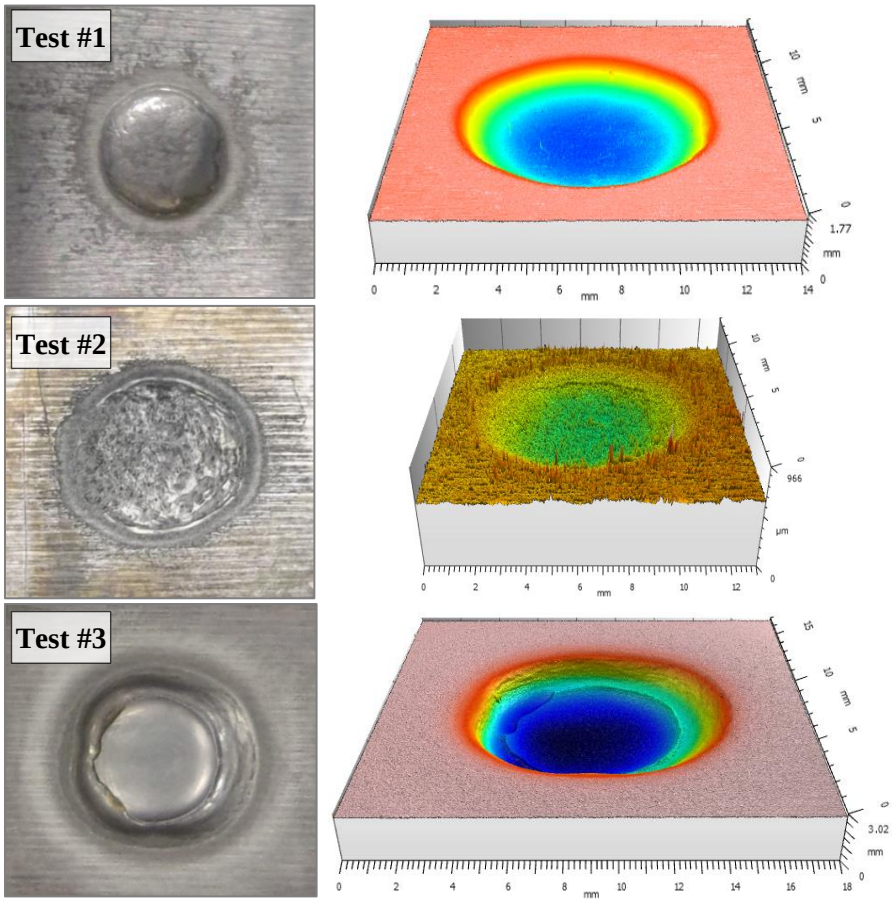

Figure 8. Photographs and optical profilometry scans of the machined indentations from tests #1 through #3. The color map for each scan is independently scaled.

Simulated vs Experimental ECM Profiles

Square Cross-Flow Tool. The time point in the simulation providing a line profile most closely matching the optical profilometry data was identified by minimizing the sum-squared deviation of the various simulated and measured depth profiles. These profiles are plotted in Figure 10; as can be seen, they fall substantially atop one another, providing preliminary validation of the primary current distribution modeling approach for prediction of ECM surface profiles. The differences between the simulation parameters and the experimental conditions invalidate the predictive capacity of the model in this case, however.

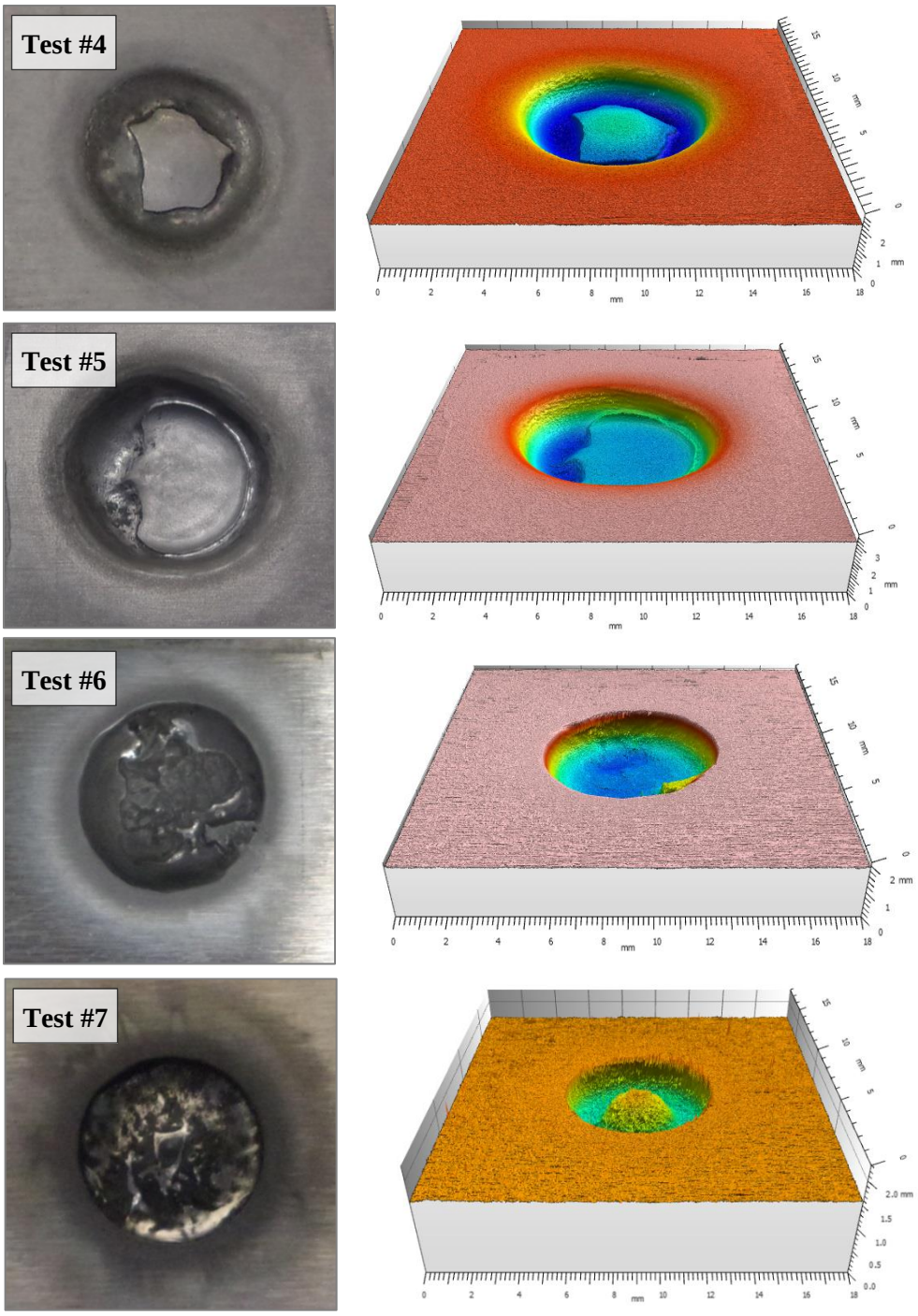

Figure 9. Photographs and optical profilometry scans of the machined indentations from tests #4 through #7. Note the convex profile of the interior region obtained with the tube tool (tests #4 and #7), as contrasted with the flat profile obtained with the rod tool (tests #5 and #6). The color map for each scan is independently scaled.

Rod Tool – Preliminary Test. As the first step in comparing the current experimental data with the primary current distribution modeling, simulated ECM profiles for the conditions of test #2 were generated (Figure 11). Comparisons to measured profiles are shown both for parallel (thick red and thin blue traces) and perpendicular (thick green and

thin purple traces) cross-sections of the machined indentations at two different simulated processing times, 1.75 min and 4.3 min. As can be seen, the simulations predict machining profiles with steeper side walls than were actually observed in the experimental data, likely due to the "active" nature of the NaCl electrolyte used (see Table I). As well, the simulations predict a higher linear machining rate than was actually achieved. In fact, whereas the tool contacted the part at $t = 4.3$ min in the experimental test, an appreciable gap still remained in the simulation at that elapsed time. Both of these variations (viz., in the linear machining rates and in the qualitative ECM profiles) can likely be explained by limitations in the simple electrochemical model used for these preliminary simulations. In particular, the relatively low flow rate attained in this test configuration (< 1 gal min^{-1}) may have led to imperfect "cleansing" of the electrode surfaces and elevated *in situ* surface resistances there. This hypothesis is supported by observations of weakly attached black residues, probably carbonaceous, left on both the part and the tool after processing. A more advanced ECM apparatus capable of operation at higher pressure and flow rate, such as that used for the prior collaborative die-sink activity with the IBR manufacturer, would likely alleviate or avoid this phenomenon, leading to higher material removal rates. Alternatively (or additionally), the model could be augmented to account for the surface effects of a flow-dependent residue layer or other phenomena.

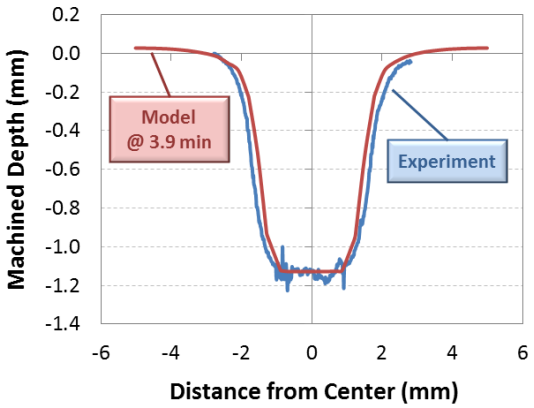

Figure 10. Measured and simulated depth profiles of the die-sink ECM part fabricated in a prior activity.

Rod Tool – Standardized Tests. On the whole, the primary current distribution simulations of the standardized ECM tests with the rod tool matched the measured profiles well, after considering the above-noted irregularities arising from the experimental apparatus. Figures 12 and 13 provide comparisons of simulated and measured profiles from tests #5 and #6, respectively, with traces included both parallel and perpendicular to the flow direction. The primary current distribution simulations provided a superb representation of the profile generated in the $NaNO_3$ electrolyte, whereas the profiles machined with NaCl matched somewhat less well. As with test #2 above, it is likely that the higher "activity" of NaCl in ECM is responsible for this deviation, including the same tendency toward a shallower slope to the machined sidewalls as observed in test #2. Both electrolytes showed faster machining on the inlet side of the part, which is consistent with the hypothesis noted above that faster flow (and thus greater local shear stress) leads to more efficient 'cleansing' of residues from the part surface, in turn leading to higher local currents in these regions.

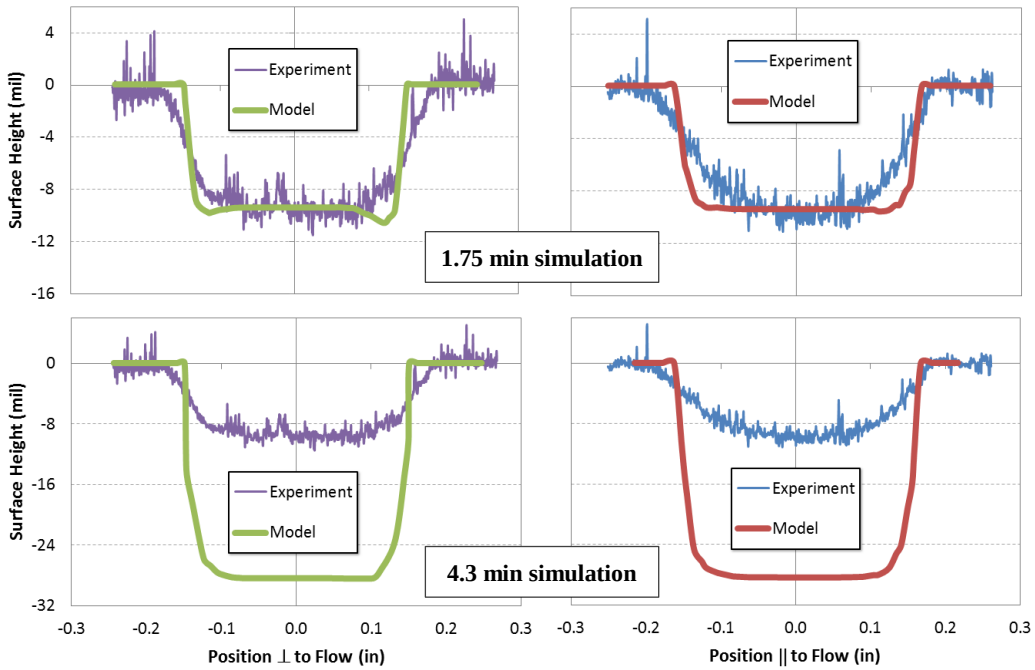

Figure 11. Measured and simulated ECM contours for test #2. Traces were recorded perpendicular (thick/thin) and parallel (thick/thin) to the flow beneath the rod tool. Note the significant difference in scales between the y-axes for all plots.

Tube Tool – Standardized Tests. The primary current distribution simulations of the indentations fabricated using the tube tool proved less successful at reproducing the experimentally-observed profiles in both electrolytes, as can be seen in Figures 14 and 15. As with the rod tool, the greater activity of NaCl as compared to $NaNO_3$ is readily apparent from the significantly greater depth and width of etch in the test with the former electrolyte. In both runs, the observed machining rate near the face of the tube tool (i.e., at $\pm$ $^{1}/_{8}$″ from the centerline) was substantially greater relative to the rate near the center of the machining region, as compared to primary current distribution predictions. The most likely explanation of this deviation is due to the neglect of flow in the model. It is somewhat unclear, though, whether the effect of flow would enter more significantly as a tertiary current distribution effect (transport of dissolved species away from the part surface) or as a 'surface cleaning' effect (removal of deposits from the machined surface). The near total lack of material removal at the centerline in the test with the $NaNO_3$ electrolyte (test #7) is especially striking, and indicates that the phenomenon causing deviation from the model was especially strong when processing with this electrolyte.

Simulated vs Experimental Current Transients

An alternative approach to gaining insight into the quality of the match between the ECM tests and primary current distribution simulations is to compare the observed and predicted current transients. Figure 16 plots the experimentally observed currents for each of the four standardized runs (tests #4 to #7) as compared to those predicted by the simulations. In all cases, the observed currents are higher than the simulations, despite the slower experimental machining rates. This discrepancy is almost certainly due to the ECM current efficiency being less than 100%: viz., oxygen evolution (reaction [4]) was

likely occurring alongside metal dissolution (Reaction [1]) to a substantial extent, which is to be expected at the 10 V_{DC} potential applied for these runs. Thus, at any practical ECM operating potential, phenomena such as surface electrochemistry will likely need to be incorporated into the model, whether in a detailed secondary current distribution form (e.g., through use of the Butler-Volmer equation) or by some semi-empirical method. Inclusion of other physics such as bubbly flow and joule heating may also be necessary.

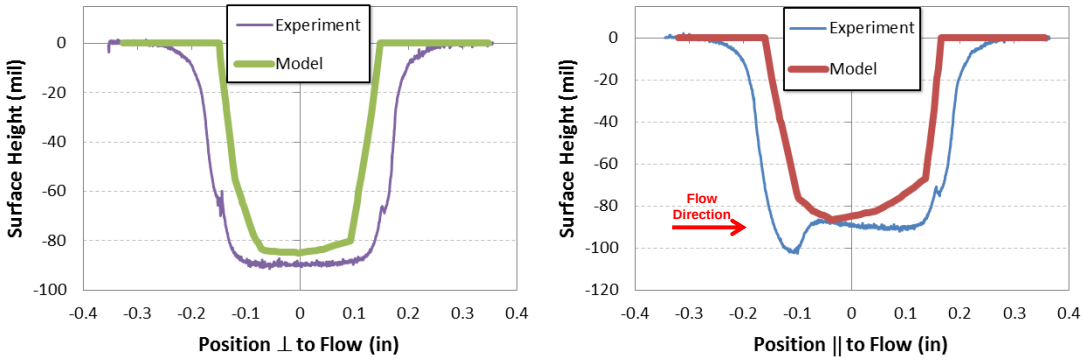

Figure 12. Measured (20 min) and simulated (14.5 min) ECM profiles from test #5 (rod tool, NaCl electrolyte).

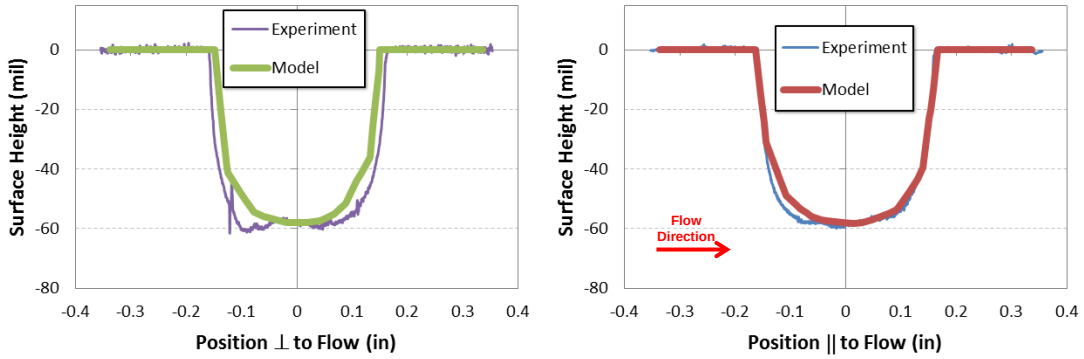

Figure 13. Measured (16 min) and simulated (9.6 min) ECM profiles from test #6 (rod tool, $NaNO_3$ electrolyte).

One encouraging aspect of this preliminary dataset lies in the similar values of the differences between the simulated versus experimental run times, (as marked in Figure 16), especially for the two runs with the tube tool. This may imply that a relatively simple linear relationship may hold between the local machining rate and one or more process parameters or physical quantities *in situ*. A more extensive dataset is required in order to draw firm conclusions, however.

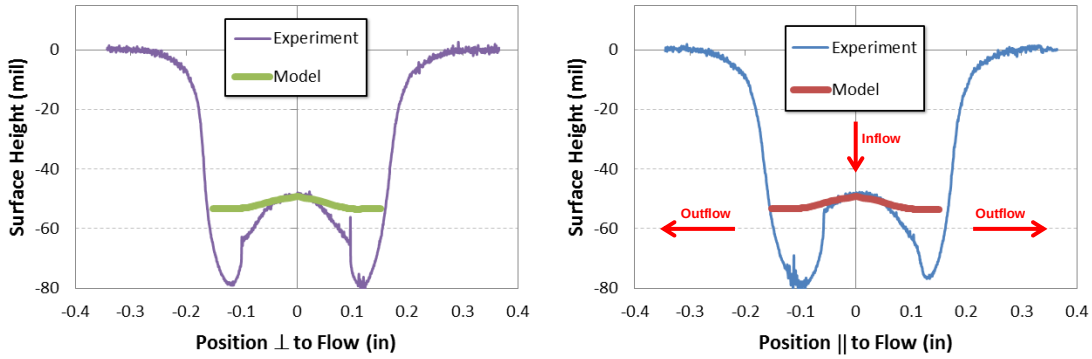

Figure 14.: Measured (20 min) and simulated (9.3 min) ECM profiles from test #4 (tube tool, NaCl electrolyte).

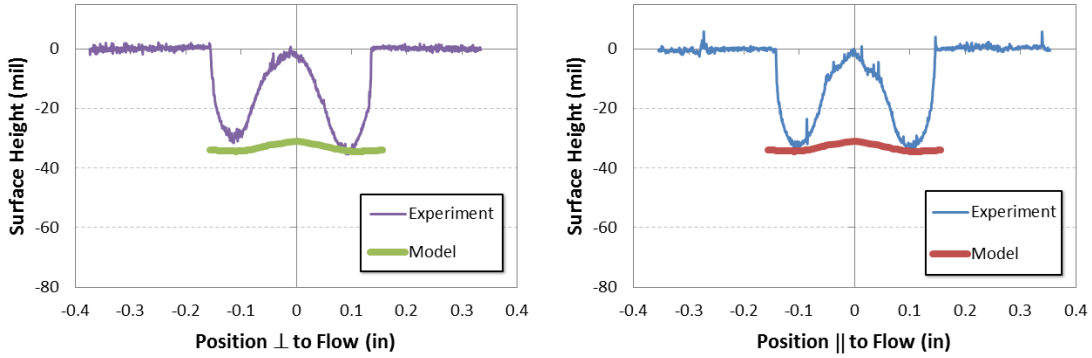

Figure 15. Measured (14 min) and simulated (6 min) ECM profiles from test #7 (tube tool, $NaNO_3$ electrolyte). The flow pattern was identical to Figure 14 (right). The simulated time used for the model profile was selected to approximately match the deepest point of etch, as the center point would have corresponded to $t \approx 0$.

Conclusions

In this work, indentations were formed in steel panels via electrochemical machining, using either a solid rod tool in a cross-flow configuration or a tube tool in a through-flow configuration. Preliminary models of these ECM operations were also constructed in COMSOL using electric field (primary current distribution) and deformable geometry physics only, omitting surface kinetics/polarization, mass/heat transfer, flow, and other phenomena. The simulated profiles were compared to optical profilometry scans of the machined indentations; as expected due to the limited physics included in these preliminary models, the quality of the model predictions varied considerably. The match between the predicted and observed indentation profiles was excellent in two of the cases examined, however. The observed asymmetry in the experimental machined profiles seems to confirm the importance of including flow effects to obtain accurate simulations, possibly including modeling local removal of accumulated deposits by surface shear, as well as suggesting a potentially significant role of the electrochemical polarization behavior in determining the spatial distribution of the material removal rate. In particular,

the current efficiency of the metal dissolution reaction likely must be considered, with the inefficient fraction of current spent to electrolyze water to oxygen gas. Future work will focus on integrating these and other physics into a robust, predictive model allowing rapid design of ECM tooling for accurate production of target part geometries with minimal prototyping and iterative development.

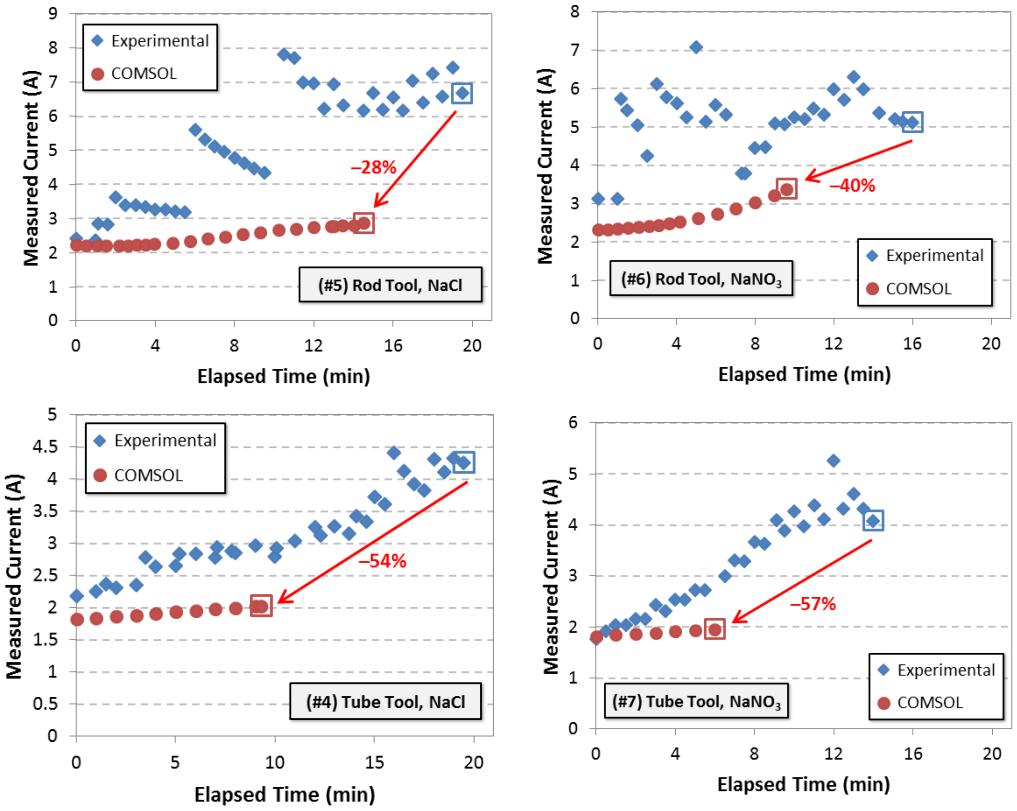

Figure 16. Plots of the measured and simulated total currents for tests #4 through #7. Tool type and electrolyte are indicated with each figure. The boxed symbols indicate the stopping point for the experimental and simulated data; the arrows and percentages indicate the extent to which the simulated time elapsed for each run was less than the actual duration of that run.

References

1. J.A. McGeough, *Advanced Methods of Machining*, p. 61, Chapman and Hall, New York (1988).
2. K.P. Rajurkar, D. Zhu, J.A. McGeough, J. Kozak, and A. De Silva, *CIRP Annals – Manufacturing Technology*, **42**(2), 567 (1999).
3. "Army Net Zero," online resource, http://www.asaie.army.mil/Public/ES/netzero/, accessed 8 Jun 2017.
4. E.J. Taylor, M.E. Inman, B.T. Skinn, T.D. Hall, S.T. Snyder, S.C. Lucatero, and E.L. Kathe, "Apparatus and Method for Recovery of Material Generated During

Electrochemical Material Removal in Acidic Electrolytes," U.S. Patent Application No. 2016/0230303 A1, dated 11 Aug 2016.

5. B. Skinn, S. Lucatero, S. Snyder, E.J. Taylor, T.D. Hall, H. McCrabb, H. Garich, and M.E. Inman, *ECS Trans*., **72**(35), 1 (2016).
6. J.A. McGeough, *Principles of Electrochemical Machining*, pp. 1-8, Halsted Press, New York (1974).
7. W.M. Deen, *Analysis of Transport Phenomena, 2nd ed.*, Oxford University Press, New York (2012).
8. F. Klocke, M. Zeis, S. Harst, A. Klink, D. Veselovac, and M. Baumgartner, *Procedia CIRP*, **8**, 265 (2013).
9. J. Kozak, K. Lubkowski, and K.P. Rajurkar, *Trans. North American Manufacturing Research Institution*, **25**, 160 (1997).
10. R. van Tijum and P.T. Pajak, *Proc. COMSOL Conference 2008 (Hannover)*, available online, https://www.comsol.com/paper/download/36405/vanTijum.pdf, accessed 8 Jun 2017.
11. K. Chikamori and S. Ito, *Denki Kagaku*, **39**, 493 (1971).